PHYSICAL REVIEW D **85,** 094016 (2012)

Analytical $\pi\pi$ scattering amplitude and the light scalars. II.

N. N. Achasov[1] and A. V. Kiselev[1,2]

[1]*Laboratory of Theoretical Physics, Sobolev Institute for Mathematics, 630090, Novosibirsk, Russia*
[2]*Novosibirsk State University, 630090, Novosibirsk, Russia*

(Received 1 February 2012; revised manuscript received 5 April 2012; published 15 May 2012)

In the paper Phys. Rev. D **83**, 054008 (2011) we constructed the $\pi\pi$ scattering amplitude T_0^0 with regular analytical properties in the s complex plane, describing both experimental data and the results based on chiral expansion and Roy equations. Now the results obtained during development of our work are presented. We dwell on questions dealing with the low $\sigma - f_0$ mixing, inelasticity description and the kaon loop model for $\phi \to \gamma(\sigma + f_0)$ reaction, and show a number of new fits. In particular, we show that the minimization of the $\sigma - f_0$ mixing results in the four-quark scenario for light scalars: the $\sigma(600)$ coupling with the $K\bar{K}$ channel is suppressed relatively to the coupling with the $\pi\pi$ channel, and the $f_0(980)$ coupling with the $\pi\pi$ channel is suppressed relatively to the coupling with the $K\bar{K}$ channel. The correct analytical properties of the $\pi\pi$ scattering amplitude are reached with the help of rather complicated background function. We also suggest much more simple background parameterization, practically preserving the resonance features, which is comfortable for experimental data analysis, but allows to describe the results based on chiral expansion and Roy equations only on the real s axis.

DOI: 10.1103/PhysRevD.85.094016 PACS numbers: 12.39.−x, 13.40.Hq, 13.66.Bc

I. INTRODUCTION

Study of light scalar resonances is one of the central problems of nonperturbative QCD; it is important for understanding the chiral symmetry realization way resulting from the confinement physics.

In 2006, we described the high-statistics KLOE data on the $\phi \to \pi^0\pi^0\gamma$ decay [1] in the frame of the kaon loop model $\phi \to K^+K^- \to (f_0 + \sigma)\gamma \to \pi^0\pi^0\gamma$ [2–6] simultaneously with the data on the $\pi\pi$ scattering and the $\pi\pi \to K\bar{K}$ reaction [7]. The chiral shielding of the $\sigma(600)$ meson [8,9] and the $\sigma - f_0$ mixing were taken into account; the analysis testified to the four-quark nature of the $\sigma(600)$ and $f_0(980)$.

At the same time in Ref. [10] the $\pi\pi$ scattering amplitude in the s complex plane was calculated with the help of chiral expansion and Roy equations. The σ pole was obtained at

$$M_\sigma = 441^{+16}_{-8} - i272^{+9}_{-12.5}\ \text{MeV}. \tag{1}$$

To compare the results of our approach and Ref. [10], we built up the S-wave $\pi\pi$ scattering amplitude T_0^0 (with $I = 0$) with correct analytical properties in the complex s plane [11]. In our model the S matrix of the $\pi\pi$ scattering is the product of the ''resonance'' and ''elastic background'' parts:

$$S_0^0 = S_0^{0\text{back}} S_0^{0\text{res}}, \tag{2}$$

and we introduced the special $S_0^{0\text{back}}$ parametrization to obtain the correct T_0^0 analytical properties ($S_0^{0\text{res}}$ had correct analytical properties in Refs. [7] already). In Ref. [11] we successfully described the experimental data and the Ref. [10] results on the real s axis using the constructed $\pi\pi$ amplitude, while the σ pole was located rather far from the Ref. [10] result.

In this paper we present the enlarged data analysis. We dwell on the minimization of the $\sigma - f_0$ mixing that leads to the four-quark scenario for light scalars: the $\sigma(600)$ coupling with the $K\bar{K}$ channel is suppressed relatively to the coupling with the $\pi\pi$ channel, and the $f_0(980)$ coupling with the $\pi\pi$ channel is suppressed relatively to the coupling with the $K\bar{K}$ channel [12]. Inelasticity is also crucial for the analysis. Here we describe the peculiar behavior of the data up to 1.2 GeV.

In Refs. [7,11] we used the factor P_K, caused by the elastic $K\bar{K}$ background phase, that allows to correct the kaon loop model, suggested in Ref. [2], under the $K\bar{K}$ threshold. Now we investigate how small this correction may be.

The set of new fits (Figs. 1–7 and tables (Tables I, II, and III) is presented in Sec. II. The residues of the $\pi\pi$ scattering amplitude and its resonance part in resonance poles are presented for the first time. The modification of the $K\bar{K}$ background phase is also described in this section.

As the analytical background $S_0^{0\text{back}}$ is a rather complicated function, in Sec. III we suggest much more simple background parameterization, practically preserving the resonance features, which is comfortable for experimental data analysis, though allows to describe the results of Ref. [10] only on the real s axis.

The conclusion is in Sec. IV.

Note that the $S_0^{0\text{res}}$ parameterization and the ''complicated'' background parameterization are the same as in Ref. [11], Secs. II and III correspondingly. All the formulas and constants, that are not defined here, may be found in Ref. [11]. Namely, the masses m_R and coupling constants g_{Rab} of resonances are defined in Eqs. (8) and (13) of Ref. [11], and at the end of page 2 together with the

coefficients x_{f_0} and x_σ. The constant $C_{f_0\sigma}$ is defined there after Eq. (7). The additional phase δ is found in Eq. (3), and the a_0^0 is the $\pi\pi$ scattering length. Parameters of the complicated background a_i, α_i, c_i, m_i, g_i are defined in Eqs. (36), (39), and (40) of Ref. [11], and the ones Λ, k_2, β, γ_i, m_{iA}, g_{iA} are defined in Eqs. (40), (43), and (46).

II. DATA ANALYSIS, BACKGROUND WITH THE CORRECT ANALYTICAL PROPERTIES (COMPLICATED BACKGROUND)

The measure of the $\sigma - f_0$ mixing intensity is the deviation from the ideal picture, when the $\pi\pi$ scattering phase δ_0^0 is equal to 90° at the $\sigma(600)$ mass m_σ, and equal to 270° at the $f_0(980)$ mass m_{f_0}. We require these phases, $\delta_0^0(m_\sigma)$ and $\delta_0^0(m_{f_0})$, to be close to their "ideal" values.

We remind that the background phase of the $K\bar{K}$ scattering, $\delta_B^{K\bar{K}}$, changes the modulus of the $K\bar{K} \to \pi^0\pi^0$ amplitude under the $K\bar{K}$ threshold, at $m < 2m_K$, in the amplitude $\phi \to K\bar{K} \to \pi^0\pi^0\gamma$ [13]. In Ref. [11] we define

$$P_K = \begin{cases} e^{i\delta_B^{K\bar{K}}} & m \geq 2m_K; \\ \text{analytical continuation of} e^{i\delta_B^{K\bar{K}}} & m < 2m_K. \end{cases} \quad (3)$$

In the present paper we investigate the influence of P_K on the $\phi \to (f_0 + \sigma)\gamma$ amplitude in the $f_0(980)$ region, $m > 850$ MeV. We upgrade the parametrization of the $\delta^{K\bar{K}}(m)$, used in Refs. [7,11]. Now the $\delta_B^{K\bar{K}}$ is parametrized in the following way:

$$e^{2i\delta_B^{K\bar{K}}} = \frac{1 + i2p_K f_K(m^2)}{1 - i2p_K f_K(m^2)}, \qquad p_K = \frac{1}{2}\sqrt{m^2 - 4m_{K^+}^2},$$
$$f_K(m^2) = -\left(1 - w + w\frac{(m - m_2)^2/\Lambda_2^2}{1 + (m - m_2)^2/\Lambda_2^2}\right) \times \frac{\arctan(\frac{m^2 - m_1^2}{\Lambda_1^2}) - \phi_0}{\Lambda_K}. \quad (4)$$

Note that the P_K also provides pole absence in the analytical continuation of the $\phi \to (f_0 + \sigma)\gamma$ amplitude under the $\pi\pi$ threshold; see Ref. [7].

The experimental data on the inelasticity η_0^0, see Fig. 4, favor the low value near 1.01 GeV and sharp growth up to 1.2 GeV. Below it is shown that it is possible to reach such a behavior.

Our results for Fits 1–5 are shown in Tables I, II, and III and Figs. 1–7. Note that the background parameters are

TABLE I. Properties of the resonances and main characteristics are shown. The resonance masses m_R and widths $\Gamma_R(m_R)$ (which may be called Breit-Wigner masses and widths) are parameters in the resonance propagators; see Ref. [11]. They have clear physical meaning in contrast to the resonance poles in the complex plane.

Fit	1	2	3	4	5
m_{f0}, MeV	978.30	974.78	981.49	979.85	980.40
$g_{f_0K^+K^-}$, GeV	3.54	4.34	5.01	5.01	7.33
$g^2_{f_0K^+K^-}/4\pi$, GeV^2	1	1.5	2	2	4.2782
$g_{f_0\pi^+\pi^-}$, GeV	−1.3924	−1.6150	−1.9836	−1.6455	−2.5874
$g^2_{f_0\pi^+\pi^-}/4\pi$, GeV^2	0.154	0.208	0.313	0.215	0.533
x_{f_0}	0.6367	0.6039	1.1701	0	1.1972
$\Gamma_{f_0}(m_{f_0})$, MeV	56.7	76.6	114.8	79.1	195.5
m_σ, MeV	479.40	471.89	470.87	472.87	469.94
$g_{\sigma\pi^+\pi^-}$, GeV	2.6676	2.6614	2.7190	2.7093	2.7362
$g^2_{\sigma\pi^+\pi^-}/4\pi$, GeV^2	0.564	0.569	0.588	0.584	0.596
$g_{\sigma K^+K^-}$, GeV	0.553	0.101	0.279	0.274	0.149
$g^2_{\sigma K^+K^-}/4\pi$, GeV^2	0.001	0.048	0.006	0.006	0.002
x_σ	1.1822	0.9187	1.7336	0	1.6291
$\Gamma_\sigma(m_\sigma)$, MeV	362.1	363.2	379.5	376.0	384.7
$C_{f_0\sigma}$, GeV^2	0.05120	0.04465	0.01307	0.00167	0.03345
δ, °	−64.69	−58.7	−64.6	−55.4	−44.0
a_0^0, m_π^{-1}	0.223	0.220	0.224	0.223	0.225
Adler zero in $\pi\pi \to \pi\pi$	(93.5 MeV)^2	(85.6 MeV)^2	(96.8 MeV)^2	(94.6 MeV)^2	(92.3 MeV)^2
$\delta_0^{0\text{res}}(m_\sigma)$, °	91.8	94.1	91.0	90.6	92.3
$\delta_0^{0\text{res}}(m_{f_0})$, °	250.1	250.1	260.1	255.1	258.7
η_0^0(1010 MeV)	0.55	0.52	0.51	0.51	0.51
χ^2_{phase} (44 points)	53.1	48.9	42.0	40.0	55.1
χ^2_{sp} (18 points)	21.2	20.8	21.3	17.0	12.6

TABLE II. The σ (600) poles (in MeV), the residues of T_0^0, Res T_0^0, and of the resonance part $T_0^{0\,\mathrm{Res}}$, Res $T_0^{0\,\mathrm{Res}}$, (in 0.01 GeV^2) in this pole on different sheets of the complex s plane depending on sheets of polarization operators $\prod ab\ (s)$ are shown.

Sheets of $\prod ab$						Fit I			Fit 5	
$\prod \pi\pi$	$\prod K\bar{K}$	$\prod \eta\eta$	$\prod \eta\eta'$	$\prod \eta'\eta'$	σ pole	Res T_0^0	Res $T_0^{0\,\mathrm{Res}}$	σ pole	Res T_0^0	Res $T_0^{0\,\mathrm{Res}}$
II	I	I	I	I	$565-204i$	$-2+14i$	$-22-11i$	$566-201i$	$-1+13i$	$-20-12i$
II	II	I	I	I	$612-346i$	$5+3i$	$-18+14i$	$569-267i$	$3+10i$	$-26-1i$
II	II	II	I	I	$542-396i$	$-1+3i$	$-16-3i$	$522-379i$	$-2+3i$	$-14-6i$
II	II	II	II	I	$577-522i$	$0.2+1i$	$-15-1i$	$612-626i$	$0.3+0.4i$	$-15-4i$
II	II	II	II	II	$633-534i$	$1+1i$	$-23+2i$	$644-651i$	$0.5+0.3i$	$-19-4i$
Sheets of $\prod ab$						Fit 3			Fit 4	
$\prod \pi\pi$	$\prod K\bar{K}$	$\prod \eta\eta$	$\prod \eta\eta'$	$\prod \eta'\eta'$	σ pole	Res T_0^0	Res $T_0^{0\,\mathrm{Res}}$	σ pole	Res T_0^0	Res $T_0^{0\,\mathrm{Res}}$
II	I	I	I	I	$572-206i$	$-2+14i$	$-21-12i$	$579-216i$	$-3+15i$	$-23-12i$
II	II	I	I	I	$572-279i$	$3+10i$	$-26+2i$	$579-273i$	$1+12i$	$-27-1i$
II	II	II	I	I	$526-395i$	$-2+2i$	$-12-5i$	...	...	...
II	II	II	II	I	$623-651i$	$0.3+0.3i$	$-14-3i$	...	...	...
II	II	II	II	II	$683-679i$	$1+0.1i$	$-19-4i$	...	...	...

located in the Appendix. Fits 1–5 show that the allowed range of $\sigma(600)$ and $f_0(980)$ parameters is rather wide. For example, $g^2_{f_0K^+K^-}/4\pi$ is 1 GeV^2 in Fit 1 and more than 4 GeV^2 in Fit 5. This result may be important for coordination of the $g^2_{f_0K^+K^-}/4\pi$ and $g^2_{a_0K^+K^-}/4\pi$ [14].

Note that in Fit 4 the $\sigma(600)$ and $f_0(980)$ are coupled only with the $\pi\pi$ channel and the $K\bar{K}$ channel ($x_{f_0} = x_\sigma = 0$). As seen from Table I and Figs. 1–7, Fit 4 is in excellent agreement with the data and the [10] results.

As it was found a long time ago, the sharp bend of the inelasticity near $\eta\eta$ threshold is caused by the $f_0(980)$ coupling to the $\eta\eta$ channel [15], and this is supported by our analysis. Rather large couplings of the f_0 to the $\eta'\eta$ or $\eta'\eta'$ are seen only indirectly (virtually) in different quantities, because the f_0 is far below their thresholds (1.5 GeV and 1.9 GeV). In our case $g_{f_0\eta\eta'}$ and $g_{f_0\eta'\eta'}$ contribute to $\sigma - f_0$ mixing and propagators. In addition, in the well-known $\eta' \to \eta\pi\pi$ decay the tail of $f_0(980)$ gives contribution due to $g_{f_0\eta\eta'}$. Note that in the $q\bar{q}$ model f_0 has rather large coupling to the $\eta'\eta$ and $\eta'\eta'$, too.

We introduce 56 parameters, but for restrictions (expressing 5 parameters through others) and parameters (or their combinations) that go to the bound of the permitted range (9 effective links), the effective number of free parameters is reduced to 42. However, it is significant that fits describe as the experimental data (65 points), as well as the $\pi\pi$ amplitude from [10] in the range $-5m_\pi^2 < s < 0.64$ GeV^2, which is treated along with experimental data.

As in [11] we show resonance poles of the T_0^0 on some unphysical sheets of its Riemannian surface, depending on sheets of the polarization operators $\Pi_R^{ab}(s)$. For this choice of sheets the imaginary parts of pole positions M_R would be connected to the full widths of the resonances ($2\,\mathrm{Im}M_R = \Gamma_R = \sum_{ab}\Gamma(R \to ab)$) in case of metastable

TABLE III. The f_0 (980) poles (in MeV), the residues of T_0^0, Res T_0^0, and of the resonance part $T_0^{0\,\mathrm{Res}}$, Res $T_0^{0\,\mathrm{Res}}$, (in 0.01 GeV^2) in this pole on different sheets of the complex s plane depending on sheets of polarization operators $\prod ab\ (s)$ are shown.

Sheets of $\prod ab$						Fit 1			Fit 5	
$\prod \pi\pi$	$\prod K\bar{K}$	$\prod \eta\eta$	$\prod \eta\eta'$	$\prod \eta'\eta'$	f_0 pole	Res T_0^0	Res $T_0^{0\,\mathrm{Res}}$	f_0 pole	Res T_0^0	Res $T_0^{0\,\mathrm{Res}}$
II	I	I	I	I	$986-26i$	$6-2i$	$-7+2i$	$986-21i$	$5-1i$	$-6+0.1i$
II	II	I	I	I	$913-302i$	$10+5i$	$-19-19i$	$1575-553i$	$-8-4i$	$-21-23i$
II	II	II	I	I	$966-450i$	$3-1i$	$-12-10i$	$2101-1065i$	$0.1+5i$	$-28-10i$
II	II	II	II	I	$962-465i$	$3-0.3i$	$-12-12i$	$2173-1158i$	$1+5i$	$-25-11i$
II	II	II	II	II	$954-586i$	$1+0.4i$	$-3-14i$	$2452-1570i$	$3+3i$	$-22-10i$
Sheets of $\prod ab$						Fit 3			Fit 4	
$\prod \pi\pi$	$\prod K\bar{K}$	$\prod \eta\eta$	$\prod \eta\eta'$	$\prod \eta'\eta'$	f_0 pole	Res T_0^0	Res $T_0^{0\,\mathrm{Res}}$	f_0 pole	Res T_0^0	Res $T_0^{0\,\mathrm{Res}}$
II	I	I	I	I	$986-23i$	$6-1i$	$-6+1i$	$985-20i$	$5-1i$	$-5+1i$
II	II	I	I	I	$1149-485i$	$3-6i$	$-14-16i$	$1187-618i$	$0.5-2i$	$-11-9i$
II	II	II	I	I	$1441-835i$	$-3+0.4i$	$-20-7i$	...	...	...
II	II	II	II	I	$1469-885i$	$-2+0.4i$	$-16-9i$	...	...	...
II	II	II	II	II	$1607-1182i$	$-1+1i$	$-11-8i$	...	...	...

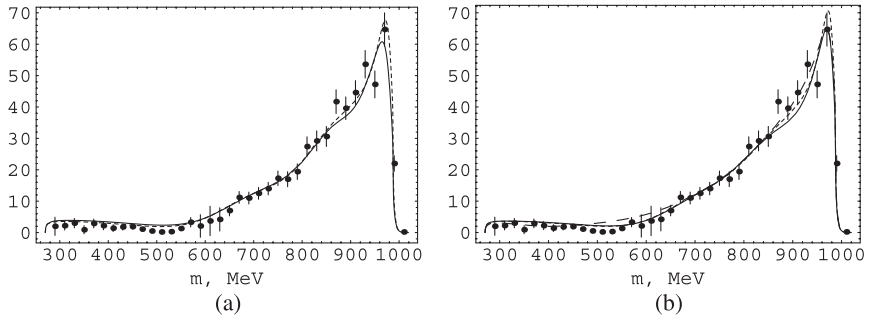

FIG. 1. The $\pi^0\pi^0$ spectrum in the $\phi \to \pi^0\pi^0\gamma$ decay, theoretical curves, and the KLOE data (points) [1] are shown: (a) Fits 1 (solid line), 5 (short-dashed line); (b) Fits 3 (solid line), 4 (short-dashed line), 6 (dashed line). Note that Fit 2 and Fit 1 curves are very close.

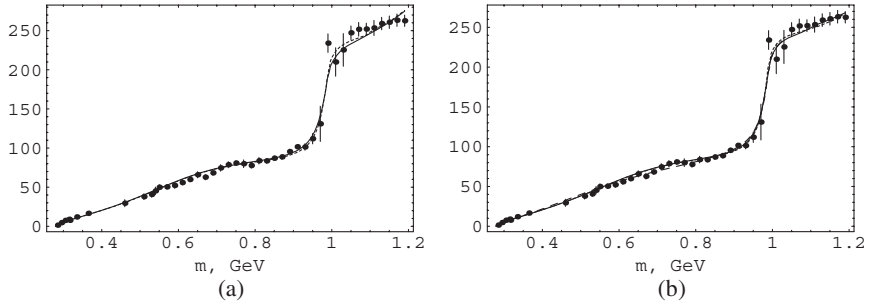

FIG. 2. The phase δ_0^0 of the $\pi\pi$ scattering (degrees) is shown: (a) Fits 1 (solid line), 5 (short-dashed line); (b) Fits 3 (solid line), 4 (short-dashed line), 6 (dashed line). Note that Fit 2 and Fit 1 curves are very close. The experimental data are from Refs. [16–20].

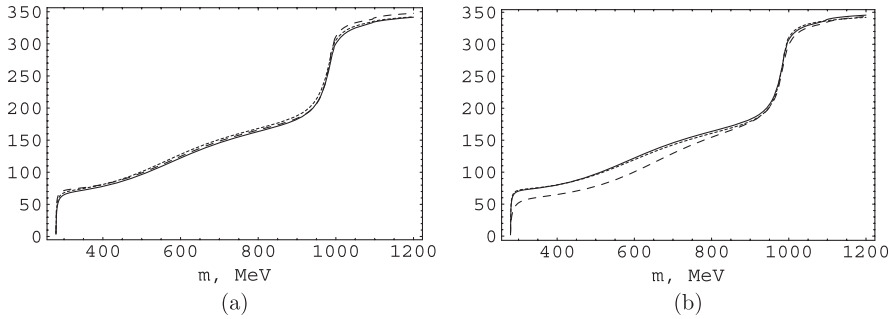

FIG. 3. The resonance phase of the $\pi\pi$ scattering $\delta_0^{0\text{res}}$ (degrees) is shown: (a) Fits 1 (solid line), 2 (short-dashed line), 5 (dashed line); (b) Fits 3 (solid line), 4 (short-dashed line), 6 (dashed line).

states, decaying to several channels. Note also that we do not show poles for Fit 2.

One can see that the obtained $\sigma(600)$ pole positions lie rather far from Eq. (1) as in our previous paper [11].

As it was shown in the $SU(2) \times SU(2)$ linear σ model, Ref. [9], the residue of the σ pole in the amplitude of the $\pi\pi$ scattering can not be connected to coupling constant in the Hermitian (or quasi-Hermitian) Hamiltonian for it has a large imaginary part. Here we calculate the residues of the amplitude T_0^0 in the $\sigma(600)$ pole (see Table II) and illustrate this fact in our case. Note that large imaginary part is both in the residues of the full amplitude T_0^0 and its resonance part $T_0^{0\text{Res}}$. So, considering the residue of the σ pole in T_0^0 or $T_0^{0\text{Res}}$ as proportional to the square of its coupling constant to the $\pi\pi$ channel is not a clear guide to understanding the σ meson nature.

The point is that there is the σ field (blurred package), and the mass and width of the $\sigma(600)$ are defined from the zero of the real part of the σ propagator denominator, and width is obtained from the imaginary part of this denominator in this point. This is a reasonable generalization of the ''Breit-Wigner'' masses and widths for the wide resonances. It is clear that the phase of the propagator passes 90° at the Breit-Wigner mass. One can see from Table I that Breit-Wigner masses of σ and f_0 are stable from Fit 1 to Fit 5.

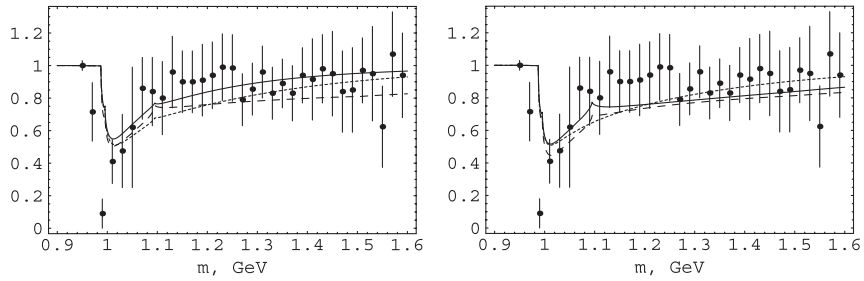

FIG. 4. The inelasticity η_0^0 is shown: (a) Fits 1 (solid line), 2 (short-dashed line), 5 (dashed line); (b) Fits 3 (solid line), 4 (short-dashed line), 6 (dashed line). The experimental data is from Ref. [16].

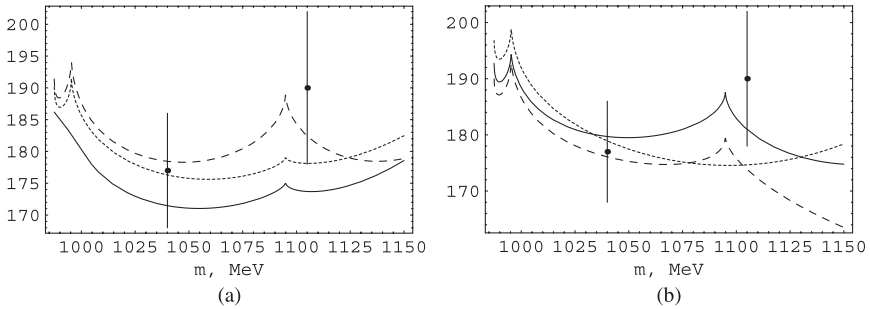

FIG. 5. The phase $\delta^{\pi K}$ of the $\pi\pi \to K\bar{K}$ scattering is shown: (a) Fits 1 (solid line), 2 (short-dashed line), 5 (dashed line); (b) Fits 3 (solid line), 4 (short-dashed line), 6 (dashed line). The experimental data are from Ref. [27].

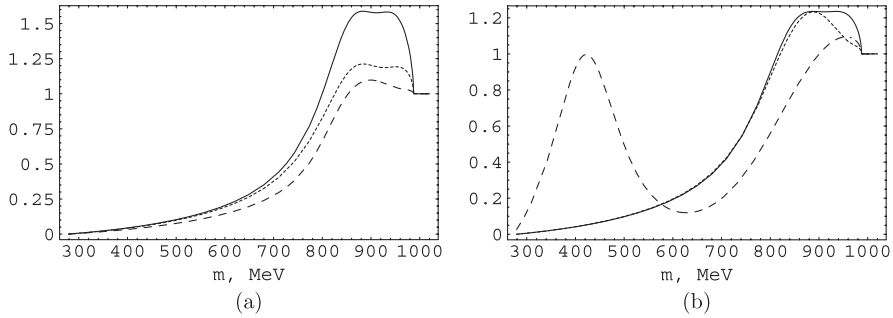

FIG. 6. The $|P_K(m)|^2$ is shown, see Eq. (7): (a) Fits 1 (solid line), 2 (short-dashed line), 5 (dashed line); (b) Fits 3 (solid line), 4 (short-dashed line), 6 (dashed line).

One can see from Fig. 6 that for Fits 2–5 with $g^2_{f_0K^+K^-}/4\pi \geq 1.5$ GeV^2 the maximum of the $|P_K|^2$ is close to 1 (about 1.2); this means that the correction to the kaon loop model [2] is small. For lower $g^2_{f_0K^+K^-}/4\pi$ the $|P_K|^2$ increases as a compensation; see Fit 1 and Fig. 6 (a). This results in a model dependence of the constant determination. A precise measurement of the inelasticity η_0^0 would resolve this problem.

One can see from Table I that for all Fits 1–5 the resonance phase $\delta^{\rm res}(m)$ is close to 90° at m_σ and to 270° at m_{f_0}; see also Fig. 3.

III. SIMPLE BACKGROUND

The background function, suggested in Ref. [11] to reach the correct analytical properties of the $\pi\pi$ scattering amplitude and used above, is rather complicated and costly in computation. In this section we suggest much more simple background parameterization, practically preserving the resonance features, which is comfortable for experimental data analysis and allows to describe the results [10] on the real s axis.

This background function is an upgrade of the one used in Ref. [7]:

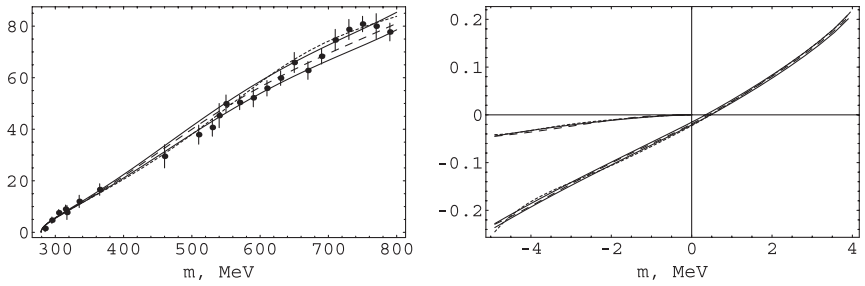

FIG. 7. (a) The phase δ_0^0 of the $\pi\pi$ scattering is shown. The solid lines mark borders of the corridor [10], and points are the experimental data from Refs. [16–20,28,29]. Fit 3 is shown with the short-dashed line, Fit 6 is shown with dashed line. Fits 1, 2, 4, 5 are very close to Fit 3 curve; (b) The real and the imaginary parts of the amplitude T_0^0 of the $\pi\pi$ scattering are shown. The solid lines mark borders of the real part corridor and the imaginary part for $s < 0$ [10]. Fit 3 is shown with the short-dashed line, Fit 6 is shown with dashed line. Fits 1, 2, 4, 5 are very close to Fit 3 curve.

$$\tan(\delta_B^{\pi\pi}) = -\frac{p_\pi}{m_\pi}\frac{b_0 - b_1\frac{p_\pi^2}{m_\pi^2} + b_2\frac{p_\pi^4}{m_\pi^4} + b_3\frac{p_\pi^6}{m_\pi^6} + \frac{m}{m_\pi}\left(c_0 + c_1\frac{p_\pi^2}{m_\pi^2} + c_2\frac{p_\pi^4}{m_\pi^4} + c_3\frac{p_\pi^6}{m_\pi^6}\right)}{(1 + 4p_\pi^2/\Lambda_1^{\pi 2})(1 + 4p_\pi^2/\Lambda_2^{\pi 2})}. \quad (5)$$

Here, $p_\pi = \sqrt{m^2 - 4m_\pi^2}/2$. Note that in comparison with Ref. [7] the function (5) has a left cut.

Let us build the χ^2 function. It may be divided into 3 parts:

$$\chi^2 = \chi^2_{\text{data}} + \chi^2_{\text{Roy}} + \chi^2_{\text{restr}},$$

where the first one is the usual χ^2 function for the experimental data, the second one provides the description of the results [10], and the third one provides the restrictions.

The χ^2_{data} is constructed with the help of the same data, as in Ref. [11], except the δ_0^0 data in the region $2m_\pi < m < 800$ MeV, where we use the [10] results. Note that in Table I we show χ^2_{phase}, obtained in the full region $2m_\pi < m < 1200$ MeV with the "old data" [16–20].

The χ^2_{Roy} is caused by the real and imaginary parts of the $T_0^0(m)$ contributions in the region $-5m_\pi^2 < s < 4m_\pi^2$, and the δ_0^0 contribution from the region $4m_\pi^2 < s < (800\ \text{MeV})^2$. Here for $\text{Re}T_0^0$ and δ_0^0 we used points and errors, and for ImT_0^0 the approximate curve $ImT_0^0(m) = -0.0327(m/2m_\pi)^3$, obtained using Fig. 1 in Ref. [10], providing us with central values, and the error is assumed to be 25%. Note that for ImT_0^0 we used the "reper" points $s = -(30\ \text{MeV})^2$, $-(50\ \text{MeV})^2$, $-(100\ \text{MeV})^2$, $-(150\ \text{MeV})^2$, $-(200\ \text{MeV})^2$, $-(250\ \text{MeV})^2$, $-(280\text{MeV})^2$, $-(308.95\ \text{MeV})^2$. The last is the end of the domain of validity of the Roy equations, connected with the Lehmann-Martin ellipse; see [10].

We impose the following set of restrictions, contributing to χ^2_{restr}:

(1) $85° < \delta_0^{0\text{res}}(m_\sigma) < 95°$ and $250° < \delta_0^{0\text{res}}(m_{f_0}) < 290°$ to provide small $\sigma - f_0$ mixing, a kind of diagonalization that results in the four-quark model scenario.

(2) $1.2 > |P_K|^2 > 0.8$ for $m > 850$ MeV. The maximum is found dynamically (at every calculation of the χ^2 function); the minimum in our situation is at 850 MeV.

(3) $-0.1 > \delta > -1.5$, trying to be not far from the result [21].

(4) $0.1 < w < 1$; 0.1 GeV $< m_2 <$ 1.5 GeV; 0.5 GeV $< \Lambda_1 <$ 2.2 GeV; 65 MeV $< \Lambda_2$ to provide reasonable form of the $|P_K|^2$.

To provide, for example, the condition $\delta > -0.1$, we add to χ^2_{restr} the term

$$T = W(-\delta - 0.1 + |\delta + 0.1|)^2, \quad (6)$$

where W is the big number. So till $\delta > -0.1$ the contribution T is equal to 0, but when $-0.1 > \delta$, T becomes large and allows to fulfill the requirement $\delta > -0.1$. Our χ^2_{restr} is the sum of contributions like Eq. (6).

Using the constructed χ^2 function, we obtain Fit 6. One can see that this fit perfectly describes the experimental data and the results based on Roy equations on the real s axis; see Table IV and Figs. 1–7. Note that in Table IV the m_{f_0} and $g^2_{f_0K^+K^-}/4\pi$ errors are adduced.

To illustrate the abilities of the background (5), we perform Fit 7 with the same resonance parameters as for Fit 3. Fit 7 provides practically the same experimental data description as Fit 3. The theoretical curves for phase δ_0^0 are shown in Fig. 8(a); they are practically the same. It is obvious that both Fit 3 and Fit 7 provide practically identical mass spectrum in $\phi \to \pi^0\pi^0\gamma$ decay also. The inelasticity is exactly the same. Additionally, Fit 7 and Fit 3 provide indistinguishable curves for T_0^0 at $4m_\pi^2 > s > 0$; see Fig. 8(b).

TABLE IV. Parameters of the Fit 6 [with simple background Eq. (5)].

Fit 6			
m_{f0}, MeV	981.80 ± 1.8	Λ_K, GeV	0.8803
$g_{f0K^+K^-}$, GeV	7.3612	Λ_1, MeV	490.24
$g^2_{f0K^+K^-}/4\pi$, GeV^2	4.3120 ± 1.0	Λ_2, MeV	154.08
$g_{f0\pi^+\pi^-}$, GeV	−2.3865	m_1, MeV	754.53
$g^2_{f0\pi^+\pi^-}/4\pi$, GeV^2	0.453	m_2, MeV	422.14
x_{f0}	0.9875	w, MeV	0.999
$\Gamma_{f0}(m_{f0})$, MeV	166.1	ϕ_0	0.787
m_σ, MeV	572.25	b_0	1.41426
$g_{\sigma 0\pi^+\pi^-}$, GeV	2.91216	b_1	0.97324
$g^2_{\sigma 0\pi^+\pi^-}$, GeV^2	0.675	b_2	−1.09477
$g_{\sigma K^+K^-}$, GeV	0.4583	b_3	−0.21134
$g^2_{\sigma K^+K^-}/4\pi$, GeV^2	0.017	c_0	2.48601
x_σ	1.01775	c_1	1.02050
$\Gamma_\sigma(m_\sigma)$, MeV	387.4	c_2	0.45705
$C_{f0\sigma}$, GeV2	0.06582	c_3	0.12373
δ, °	−5.8	Λ_1^π	160.84
a_0^0, m_π^{-1}	0.220	Λ_2^π	522.98
Adler zero in $\pi\pi \to \pi\pi$	(89.8 MeV)^2	$\delta_0^{0\,\mathrm{res}}(m_\sigma)$,	93.1
χ^0_{phase} (44 points)	39.4	$\delta_0^{0\,\mathrm{res}}(m_{fo})$,	251.4
χ^2_{sp}(18 points)	13.9	η_0^0 (1010 MeV)	0.45

IV. CONCLUSION

Our investigation shows that the scenario, based on the four-quark model, completely agrees with the current experimental data and theoretical requirements. It is shown that the requirement of the weak $\sigma(600) - f_0(980)$ mixing leads to the $g_{\sigma K^+K^-}$ and $g_{f_0\pi^+\pi^-}$ suppression that is predicted by the four-quark model; see Table I.

The small ratios $(g_{\sigma K^+K^-}/g_{\sigma\pi^+\pi^-})^2$ and $(g_{f_0\pi^+\pi^-}/g_{f_0K^+K^-})^2$ (see Table I) indicate that the $q\bar{q}$ component is less than 10% in $\sigma(600)$ and less than 20% in $f_0(980)$, so the current analysis support the conclusion of Ref. [11] about the dominance of $\bar{u}\,\bar{d}\,ud$ in $\sigma(600)$ and $\bar{s}\,\bar{d}\,ds$ in $f_0(980)$.

The behavior of the factor $P_K(m)$, which corrects the kaon loop model, is model dependent. We show that for large enough $g^2_{f_0K^+K^-}/4\pi$ constant (for example, 1.5 GeV^2) the current data (including the Ref. [10] results) may be well-described with this factor close to 1 at 850 MeV $< m$, but for smaller values of this constant (for example, 1 GeV^2) the correction increases. New precise data on the $\pi\pi \to K\bar{K}$ reaction and the inelasticity (η_0^0) of the $\pi\pi$ scattering would give an ability to understand more about this factor and reduce the region of possible values of parameters.

Note that the Roy equations are not exact in principle, also as the equations for distribution functions in statistics, obtained by truncation of the Bogolyubov chain, or equations for amplitudes (Green's functions, vertices), obtained by truncation of the Schwinger-Dyson connected equations, are not exact in principle. For example, Sudakov's equation for vertex in quantum electrodynamics. The Roy

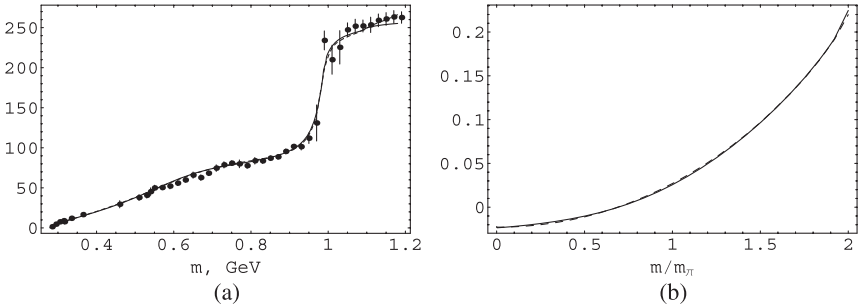

FIG. 8. The comparison of Fit 3 and Fit 7 (with the same resonance parameters, but the background parameterization (5)): (a) the phase δ_0^0; (b) the amplitude T_0^0 under the $\pi\pi$ threshold. Solid lines are Fit 7, dashed lines are Fit 3, points are the experimental data. The curves are practically the same.

TABLE V. Parameters of the $K\bar{K}$ background phase, $\delta_B^{K\bar{K}}$, are shown.

Fit	1	2	3	4	5
Λ_K, GeV	0.975	1.245	1.375	1.450	1.894
Λ_1, MeV	381.56	404.49	387.56	412.43	322.93
Λ_2, MeV	83.113	81.137	86.246	65.000	68.041
m_1, MeV	827.48	823.54	801.40	791.48	808.17
m_2, MeV	909.17	923.55	911.59	970.52	963.55
w, MeV	0.471	0.618	0.492	0.750	0.750
ϕ_0	−0.299	0.021	0.153	0.271	0.622

equation is one-channel and has a solution with the two-sheeted Riemannian surface, that is, different from solution of the exact problem, which should have an infinity-sheeted Riemannian surface.

The determination of the pole positions and their residues do not give us practically any information on the light scalars nature, because they can not be connected to coupling constants in the Hermitian (or quasi-Hermitian) Hamiltonian (see also Ref. [9]), because of large imaginary parts. Besides, the residue of the amplitude in the pole is strongly distorted by the background part of the amplitude; see Tables II and III, that give an essential contribution even for relatively narrow $f_0(980)$.

Let us dwell on the results presented in Table III. Reminding that for a stable particle with the mass m_0 there is the pole in the amplitude

$$T = -\frac{g^2/16\pi}{s - m_0^2}$$

at $s = m_0^2$, the residue of the amplitude Res$T$ is connected to the coupling constant (g) of the stable particle with the $\pi\pi$ channel.

One can see that the real part of the T_0^0 residue in the $f_0(980)$ pole is positive, so the coupling constant should be practically pure imaginary, which is physically meaningless. Note that the residue of the amplitude resonance part $T_0^{0\mathrm{Res}}$ is good. That is why the best way for understanding the nature of the light scalars is the investigation of their production mechanisms in physical processes.

The simple background parameterization, suggested in Sec. III, may be used for experimental data analysis and the description of the Ref. [10] results for real s. It is shown that the resonance features are practically preserved; moreover, one can see that for even more simple back-

TABLE VI. Parameters of the first background ($P_{\pi 1}$) (see Ref. [11]) are shown.

Fit	1	2	3	4	5
a_1	−2.767	−1.997	−2.727	−3.152	−2.320
a_2	0.00997	0.02824	0.01228	0.00995	0.00987
a_3	0	0	0	0	0
a_4	2.4774	1.1655	1.9460	3.6119	1.9579
a_1, GeV^2	430.875	−3.472	299.566	187.438	230.647
a_2, GeV^4	1038.375	802.006	1006.643	924.912	876.525
a_3, GeV^6	853.500	810.211	840.573	805.455	805.900
a_4, GeV^8	237.251	239.362	232.860	225.823	233.065
a_5, GeV^{10}	25.3514	25.4850	24.8635	24.9756	25.2960
a_6, GeV^{12}	0.248630	0.218526	0.225182	0.240893	0.224103
c_1, GeV	504.558	680.672	543.245	499.429	557.733
c_2, GeV^3	−2745.58	−2246.19	−2532.80	−2395.72	−2484.57
c_3, GeV^5	132.007	176.850	226.617	256.520	191.569
c_4, GeV^7	390.262	379.216	399.808	404.615	394.230
c_5, GeV^9	50.6689	51.7071	50.4545	49.8151	51.4728
c_6, GeV^{11}	−0.612729	−0.636956	−0.633709	−0.711296	−0.646822
m_1, MeV	921.52	766.81	1049.46	1088.06	915.18
g_1, MeV	301.06	302.40	302.30	333.34	330.83
m_2, MeV	1395.84	937.07	970.74	1104.06	1025.77
g_2, MeV	367.05	305.90	310.37	421.12	324.93
m_3, MeV	1208.42	1432.57	1098.81	1125.51	1330.56
g_3, MeV	335.62	304.46	388.57	378.42	301.39
m_4, MeV	1078.40	898.85	1053.21	1162.64	907.71
g_4, MeV	395.12	429.54	403.00	388.93	437.65
m_5, MeV	1011.58	991.70	1017.19	1051.17	1008.35
g_5, MeV	499.99	503.50	507.03	500.41	502.24
m_6, MeV	932.07	1240.82	1174.80	1154.23	1264.43
g_6, MeV	535.90	616.91	574.55	542.66	629.02

TABLE VII. Parameters of the second background ($P_{\pi 2}$) (see Ref. [11]) are shown.

Fit	1	2	3	4	5
Λ, MeV	88.506	78.187	73.302	70.443	68.804
k_2	0.0295157	0.0310661	0.0313951	0.0415406	0.0250125
β	143.367	132.832	125.729	126.711	165.179
γ_1	383.759	330.693	365.564	374.814	450.415
γ_2	21.5451	24.7134	22.9274	22.1454	23.1322
m_{1A}, MeV	687.75	668.05	721.92	837.74	607.47
g_{1A}, MeV	301.22	303.07	305.36	392.13	343.56
m_{2A}, MeV	495.44	554.28	492.36	487.79	515.18
g_{2A}, MeV	504.69	488.58	457.53	454.08	494.25
m_{3A}, MeV	631.67	637.64	625.43	599.93	675.83
g_{3A}, MeV	117.86	101.74	101.00	101.35	100.98

ground, used in Ref. [7], they changed not so much, though the Ref. [10] results were not included.

In this investigation we paid more attention to the inelasticity η_0^0, namely, we tried to reproduce the peculiar behavior near the threshold indicated by the experimental data. This behavior was discussed quite widely in Ref. [15] for the first time and then in later works, for example, in Ref. [22]. Unfortunately, the current data have large errors, so the precise measurement of the inelasticity η_0^0 near 1 GeV in $\pi\pi \to \pi\pi$ would be very important.

To reduce (if not avoid) an effect of heavier isosinglet scalars, we restrict ourselves to the analysis of the mass region $m < 1.2$ GeV, where, as one may expect, an effect of heavier scalars would not be essential. As to mixing light and heavier isosinglet scalars, this question could not be resolved once and for all at present, in particular, because their properties are not well-established up to now. A preliminary consideration (without taking into account the mixing due to common decay channels) was carried out in Ref. [23], where, in particular, it was shown that the mixing could affect the mass difference of the isospinor and isovector.

The nature of heavy scalars ($f_0(1370)$, $a_0(1450)$) is a hard question; apparently they are $q\bar{q}$ states (see Refs. [23,24]), but it should be noted that their features are not well-established, and the authors of Ref. [25] even question the very existence of such a state as $f_0(1370)$. Note that the preliminary consideration of this question may be found, for example, in Ref. [26].

ACKNOWLEDGMENTS

We thank very much H. Leutwyler for providing numerical values of the $T_0^0(s)$ on the real axis obtained in Ref. [10], useful discussions, and kind contacts. This work was supported in part by RFBR Grant No. 10-02-00016, and Interdisciplinary Project No. 102 of the Siberian division of RAS.

APPENDIX

Tables V, VI, and VII show the background parameters.

[1] A. Aloisio *et al.* (KLOE Collaboration), Phys. Lett. B **537**, 21 (2002).
[2] N. N. Achasov and V. N. Ivanchenko, Nucl. Phys.**B315**, 465 (1989).
[3] N. N. Achasov and V. V. Gubin, Phys. Rev. D **56**, 4084 (1997).
[4] N. N. Achasov and V. V. Gubin, Phys. Rev. D **63**, 094007 (2001).
[5] N. N. Achasov, Nucl. Phys.**A728**, 425 (2003).
[6] N. N. Achasov and A. V. Kiselev, Phys. Rev. D **68**, 014006 (2003).
[7] N. N. Achasov and A. V. Kiselev, Phys. Rev. D **73**, 054029 (2006); **74**, 059902 (2006); Yad. Fiz. **70**, 2005 (2007); Phys. At. Nucl. **70**, 1956 (2007).
[8] N. N. Achasov and G. N. Shestakov, Phys. Rev. D **49**, 5779 (1994).
[9] N. N. Achasov and G. N. Shestakov, Phys. Rev. Lett. **99**, 072001 (2007).
[10] I. Caprini, G. Colangelo, and H. Leutwyler, Phys. Rev. Lett. **96**, 132001 (2006).
[11] N. N. Achasov and A. V. Kiselev, Phys. Rev. D **83**, 054008 (2011).
[12] R. L. Jaffe, Phys. Rev. D **15**, 267 (1977); **15**, 281 (1977).
[13] In the kaon loop model, $\phi \to K^+K^- \to \gamma(f_0 + \sigma)$ [2–4], the amplitude of the signal $\phi(p) \to \gamma(f_0 + \sigma) \to \pi^0(k_1)\pi^0(k_2)\gamma(q)$ is

$$M_{sig} = g(m)\left((\phi\epsilon) - \frac{(\phi q)(\epsilon p)}{(pq)}\right)T(K^+K^- \to \pi^0\pi^0) \times 16\pi, \tag{7}$$

where $g(m)$ is the kaon loop function, ϕ and ϵ are polarization vectors of the ϕ meson and photon; see Refs. [7,11].

[14] These constants are equal in the naive four-quark model.
[15] N. N. Achasov, S. A. Devyanin, and G. N. Shestakov, Z. Phys. C **22**, 53 (1984).
[16] B. Hyams *et al.*, Nucl. Phys.**B64**, 134 (1973).
[17] P. Estabrooks and A. D. Martin, Nucl. Phys. **B79**, 301 (1974).
[18] A. D. Martin, E. N. Ozmutlu, and E. J. Squires, Nucl. Phys. **B121**, 514 (1977).
[19] V. Srinivasan *et al.*, Phys. Rev. D **12**, 681 (1975).
[20] L. Rosselet *et al.*, Phys. Rev. D **15**, 574 (1977).
[21] N. N. Achasov and A. A. Kozhevnikov, Phys. Rev. D **61**, 054005 (2000); Yad. Fiz. **63**, 2029 (2000); Phys. At. Nucl. **63**, 1936 (2000).
[22] R. Garcia-Martin, R. Kaminski, J. R. Pelaez, J. Ruiz de Elvira, and F. J. Yndurain, Phys. Rev. D **83**, 074004 (2011).
[23] D. Black, A. Fariborz, and J. Schechter, Phys. Rev. D **61**, 074001 (2000); A. Fariborz, R. Jora, and J. Schechter, Phys. Rev. D **79**, 074014 (2009).
[24] N. N. Achasov, Yad. Fiz. **65**, 573 (2002); Phys. At. Nucl. **65**, 546 (2002).
[25] E. Klempt and A. Zaitsev, Phys. Rep. **454**, 1 (2007).
[26] F. Giacosa, Phys. Rev. D **80**, 074028 (2009); D. Parganlija, F. Giacosa, and D. H. Rischke, Phys. Rev. D **82**, 054024 (2010).
[27] A. Etkin *et al.*, Phys. Rev. D **25**, 1786 (1982).
[28] S. Pislak *et al.*, Phys. Rev. Lett. **87**, 221801 (2001).
[29] J. R. Batley *et al.*, Eur. Phys. J. C **54**, 411 (2008).